Int. J. Adv. Appl. Math. and Mech. 10(1) (2022) 1 – 14 (ISSN: 2347-2529)

Journal homepage: www.ijaamm.com

International Journal of Advances in Applied Mathematics and Mechanics

EHD instability of two superposed couple stress viscoelastic dielectric fluids streaming through porous media of different permeabilities

Research Article

Mohamed F. El - Sayed[a, b] *, **Mohamed F. E. Amer**[b], **Zakaria S. Alfayzi**[a]

[a] *Department of Mathematics, College of Science, Qassim University, P. O. Box 6644, Buraidah 51452, Saudi Arabia*

[b] *Department of Mathematics, Faculty of Education, Ain Shams University, P. O. Box 11341, Heliopolis (Roxy), Cairo, Egypt*

Received 10 August 2022; accepted (in revised version) 01 September 2022

Abstract: Using applied electric fields that act normally on the interface between the fluids when no surface charges are present, we investigated the interface instability between two uniform semi-infinite superposed incompressible dielectric viscoelastic fluid (of the couple stress type) streams through porous media with varying permeabilities with uniform velocities and densities. Using perturbation and normal mode techniques to the governing equations of fluid motion and Maxwell's equations (in quasi-static approximation assumption forms) and the corresponding boundary conditions to obtain a dispersion relation of complicated form that cannot be solved analytically to express the growth rates in terms of wave numbers. With Mathematica and Gaster's theory, we were able to solve the problem numerically to get the growth rates in terms of wave numbers with constant values for other factors. In order to show how various parameters affect the system's stability, the visual results are presented. The stabilizing effects of velocities, kinematic viscosities, densities, and dielectric constants are discovered, while the destabilizing impacts of kinematic viscoelasticities, medium permeabilities, porous medium porosity, and electric fields are discovered. Finally, the Kelvin-Helmholtz instability is suppressed by the surface tension in the presence of couple stress fluids and applied electric fields, and this is due to the surface tension's stabilizing impact on the instability.

MSC: 76A10 • 76E25 • 76W05 • 76S05

Keywords: Hydrodynamic stability • Couple stress viscoelastic fluids; Dielectric fluids • Flows through porous media • Electrohydrodynamics

1. Introduction

In the last few decades, research on the instability of non-Newtonian fluids has grown significantly. In many viscoelastic fluids, stress-strain relationships are non-linear, making them difficult to classify. Non-Newtonian fluids, such as couple stress fluid, are one example [1, 2]. Fluids of this type can be used to describe lubricants, blood suspension fluids, metabolic difficulties, and more [3]. It has been established that synovial fluid in human joints behaves as a couple stress fluid, which has been the primary goal of scientific research [4, 5]. It is also possible to use couple stress fluids in the process to solidify liquid crystals and colloidal solutions, cool the metallic plate in a bath, or extrude polymer fluids. Understanding the nature of couple stress behavior is essential for demonstrating the mechanism of rheologically complicated fluids such as colloidal solutions, liquid crystals, polymeric suspensions, and human blood.The Stokes couple stress theory states that the rotational field in terms of the velocity field can be

* Corresponding author.
E-mail address(es): Mo.ElSayed@qu.edu.sa (Mohamed F. El - Sayed).

used to establish the stress and strain rate connection [6, 7] . Non-Newtonian fluids can be studied using a variety of methodologies, among which the couple stress fluids have distinct characteristics, such as the presence of couple stress, body couples, boundary roughness, and non-symmetric stress tensors [8] - [11]. For recent investigations about the couple stress fluids, see the studies of Kumar, and Sing [12], and Munivenkatappa et al. [13].

Flows through porous media have been a subject of great interest for the last several decades [14, 15]. Many technical applications, including as ground water hydrology, chemical catalytic reactors and ceramic processes, as well as petroleum reservoirs, ground water contamination and filtration procedures were the driving force behind this interest in geophysical thermodynamics. Much of the recent works in this topic have been reviewed by Bejan [16], Straughan [17], and Nield and Bejan [18].

Generally speaking, the Darcy's law describes what happens when a fluid passes through a porous substance. The resistance term replaces the typical viscous and couple stress viscous terms in the equation of couple stress fluid motion due to this macro law $[-k_1^{-1}(\mu-\mu'\nabla^2)\boldsymbol{q}]$, where μ and μ' are the viscosity and couple stress viscosity, k_1 is the medium permeability, and $\boldsymbol{q}$ is the Darcian (filter) velocity of the couple stress fluid in porous medium. Couple stress effects in the flow of non-Newtonian fluids through porous media have attracted a lot of attention in recent years. A growing interest in the possibilities of boosting oil recovery efficiency from water flooding projects by mobility control with non-Newtonian displacement fluids appears to be driving attention to this issue right now in oil reservoir engineering. As a result, an understanding of the stress effects of non-Newtonian displacing and displaces fluids in an oil displacement mechanism is now critical.

There are several technical processes that need the simultaneous flow of fluids with varying viscosities, elasticity, and density. Packed bed reactors, boiling in porous media, and many more processes all use these types of fluxes. Any time there is an unstable interface between two fluids, flow resistance will rise dramatically. This rise in resistance can, in turn, produce flooding in chemical reactors with counter-current packing and drying out in porous media that are heated to high temperatures. Emulsion generation is also facilitated by such instabilities in petroleum production engineering. Thus, we may estimate the limiting operating conditions of the aforesaid processes based on our understanding of the start of instability [19]-[24]. An important part of fluid mechanics, electrohydrodynamics examines the interactions between electric and hydrodynamic forces, when hydrodynamic motion is associated with electric phenomena. The equations of motion in electrohydrodynamics can be divided into two groups: hydrodynamic and electric field equations. Additionally, the equations' connection is evident in the boundary conditions [25].

Electrical fluid dynamics can be used in a wide variety of domains, such as biological electrofluid dynamics and zero-gravity liquid ejection, as well as research on liquid and gas insulations. In light of these facts, there is a growing need to study the electrohydrodynamic phenomena involving the use of non-Newtonian fluids for applications in agriculture, biomedicine, etc., because little is known about the electrohydrodynamic stability of non-Newtonian fluids because the interaction between the fluid and elasticity is extremely complicated. For an excellent review about applications of electrohydrodynamics through porous media, see the paper of Del Rio and Whitaker [26]. Applications of EHD stability of couple stress fluids streaming through porous medium has been shown by Rudraiah et al. [27], Shivakumara et al. [28], Shankar et al. [29], Rana et al. [30], El-Sayed et al. [31], and El-Sayed and Alanzi [32]. This study attempts to investigate the electrohydrodynamic stability of two superposed couple stress viscoelastic dielectric fluids streaming through porous media of different permeabilities, which, to the best of our knowledge, has never been investigated before, keeping in mind the importance and applications in modern technology of electrified couple stress fluids and flows through porous media. This article is organized as follows: In section 2, the details of the physical system and the mathematical model are presented, and the linearized model equations for the perturbed state are given together with the base state profiles. In section 3, the boundary and interfacial conditions are given and used to obtain the solutions of the differential equations of couple stress fluids and the applied electric fields. In section 4, a novel dispersion relation of complicated form has been derived, which cannot be solved analytically. Instead, we solved it numerically using Gaster's theorem [33] and Mathematica software to express the growth rates in terms of wave numbers with constant values of all other parameters, and the obtained results are shown graphically to illustrate the effects of various parameters on the stability of the system. Finally, section 5 includes the conclusions of the main obtained findings.

2. Problem formulation and perturbation equations

Consider the system of two uniform semi-infinite superposed incompressible viscoelastic dielectric fluids of couple- stress type streaming in porous media of uniform porosity ε, and different medium permeabilities $k_1^{(1)}$ and $k_1^{(2)}$. The two fluids are of uniform densities $\rho^{(1)}$ and $\rho^{(2)}$, horizontal velocities $U^{(1)}$ and $U^{(2)}$, dielectric constants $\epsilon^{(1)}$ and $\epsilon^{(2)}$, dynamic viscosities $\mu^{(1)}$ and $\mu^{(2)}$, dynamic viscoelastisities $\mu'^{(1)}$ and $\mu'^{(2)}$, separated by a horizontal interface at $z=0$. The superscripts (1) and (2) refer to the lower and upper fluid, respectively. The whole system is influenced by the presence of constant applied electric fields $E_0^{(1)}$ and $E_0^{(2)}$ acting normally (in the negative z-axis) to the direction of streaming. The kinematic viscosities and kinematic viscoelasticities of the two fluids are defined by $\nu^{(j)}=\mu^{(j)}/\rho^{(j)}$ and $\nu'^{(j)}=\mu'^{(j)}/\rho^{(j)}$, respectively, for $j=1,2$.

The governing equations in three-dimensional Cartesian coordinates are the equation of continuity, Navier-Stokes

equation of motion, and Maxwell's equations (using quasi-static approximation assumption) in both media defined by [32]

$$\nabla \cdot \boldsymbol{q}^{(j)} = 0 \tag{1}$$

$$\frac{\rho^{(j)}}{\varepsilon^2}\left[\varepsilon\frac{\partial \boldsymbol{q}^{(j)}}{\partial t} + \left(\boldsymbol{q}^{(j)}\cdot\nabla\right)\boldsymbol{q}^{(j)}\right] = -\nabla p^{(j)} + \rho^{(j)}\boldsymbol{g} - \frac{\rho^{(j)}}{k_1^{(j)}}\left(v^{(j)} - v'^{(j)}\nabla^2\right)\boldsymbol{q}^{(j)} \tag{2}$$

$$\nabla \cdot \left(\epsilon^{(j)}\boldsymbol{E}^{(j)}\right) = 0 \tag{3}$$

$$\nabla \times \boldsymbol{E}^{(J)} = 0 \quad \text{i. e.} \quad \boldsymbol{E}^{(j)} = -\nabla\Psi^{(j)} \tag{4}$$

where $\boldsymbol{q}^{(j)}$ is the fluid velocities, $p^{(j)}$ is the pressures, $\psi^{(j)}$is the electric potentials, $\boldsymbol{g} = (0,0,-g)$ is the acceleration due to gravity acting in the negative z-direction. Equations (1)-(4) occur for both regions $-\infty < z < 0$ and $0 < z < \infty$, respectively. From eqs. (3) and (4), we get

$$\nabla^2\Psi^{(j)} = 0 \tag{5}$$

Let $\boldsymbol{q}_1^{(j)}\left(u^{(j)}, v^{(j)}, w^{(j)}\right), p_1^{(j)}, \Psi_1^{(j)}$ and $\boldsymbol{E}_1^{(j)}$ denote the perturbations in fluid velocities $\boldsymbol{q}^{(j)}\left(U^{(j)},0,0\right)$, pressures $p^{(j)}$, electric potentials $\Psi^{(j)}$, and electric fields $\boldsymbol{E}^{(j)}$, in the lower and upper phases, respectively. Hence, the linearized perturbation equations of eqs. (1)-(5) reduce to

$$\frac{\partial u^{(j)}}{\partial x} + \frac{\partial v^{(j)}}{\partial y} + \frac{\partial w^{(j)}}{\partial z} = 0 \tag{6}$$

$$\frac{1}{\varepsilon^2}\left[\varepsilon\frac{\partial u^{(j)}}{\partial t} + U^{(j)}\frac{\partial u^{(j)}}{\partial x}\right] = -\frac{1}{\rho^{(j)}}\frac{\partial p_1^{(j)}}{\partial x} - \frac{1}{k_1^{(j)}}\left(v^{(j)} - v'^{(j)}\nabla^2\right)u^{(j)} \tag{7}$$

$$\frac{1}{\varepsilon^2}\left[\varepsilon\frac{\partial v^{(j)}}{\partial t} + U^{(j)}\frac{\partial v^{(j)}}{\partial x}\right] = -\frac{1}{\rho^{(j)}}\frac{\partial p_1^{(j)}}{\partial y} - \frac{1}{k_1^{(j)}}\left(v^{(j)} - v'^{(j)}\nabla^2\right)v^{(j)} \tag{8}$$

$$\frac{1}{\varepsilon^2}\left[\varepsilon\frac{\partial w^{(j)}}{\partial t} + U^{(j)}\frac{\partial w^{(j)}}{\partial x}\right] = -\frac{1}{\rho^{(j)}}\frac{\partial p_1^{(j)}}{\partial z} - \frac{1}{k_1^{(j)}}\left(v^{(j)} - v'^{(j)}\nabla^2\right)w^{(j)} \tag{9}$$

and

$$\nabla^2\Psi_1^{(1)} = 0 \quad \text{where} \quad \boldsymbol{E}_1^{(1)} = -\nabla\Psi_1^{(1)} \tag{10}$$

Analyzing the disturbance into normal modes, we seek solutions whose dependence on x, y, z and t is of the form

$$f(z)\exp\left[i\left(k_x x + k_y y + nt\right)\right] \tag{11}$$

where $f(z)$ is some function of z, and k_x, k_y are the horizontal wave numbers, such that the resultant wave number is defined by $k = \sqrt{k_x^2 + k_y^2}, i = \sqrt{-1}$, and $n = n_r + i n_i$ is the complex growth rate of the disturbance.

Substitute from eq. (11) into eqs. (6)-(10), we obtain

$$ik_x u^{(j)} + ik_y v^{(j)} + Dw^{(j)} = 0 \tag{12}$$

$$\rho^{(j)}\left\{\frac{i}{\varepsilon^2}\left(\varepsilon n + k_x U^{(j)}\right) + \frac{1}{k_1^{(j)}}\left[v^{(j)} - v'^{(j)}\left(D^2 - k^2\right)\right]\right\}u^{(j)} = -ik_x p_1^{(j)} \tag{13}$$

$$\rho^{(j)}\left\{\frac{i}{\varepsilon^2}\left(\varepsilon n + k_x U^{(j)}\right) + \frac{1}{k_1^{(j)}}\left[v^{(j)} - v'^{(j)}\left(D^2 - k^2\right)\right]\right\}v^{(j)} = -ik_y p_1^{(j)} \tag{14}$$

$$\rho^{(j)}\left\{\frac{i}{\varepsilon^2}\left(\varepsilon n+k_xU^{(j)}\right)+\frac{1}{k_1^{(j)}}\left[\nu^{(j)}-\nu'^{(j)}\left(D^2-k^2\right)\right]\right\}w^{(j)}=-Dp_1^{(j)} \tag{15}$$

and

$$\left(D^2-k^2\right)\Psi_1^{(j)}=0 \quad \text{where} \quad \mathrm{D}=\frac{\mathrm{d}}{\mathrm{dz}} \tag{16}$$

Multiply eqs. (13) and (14) by $-ik_x$ and $-ik_y$, respectively, adding the resulting two equations, and making use of eq. (12), we get

$$\rho^{(j)}\left\{\frac{i}{\varepsilon^2}\left(\varepsilon n+k_xU^{(j)}\right)+\frac{1}{k_1^{(j)}}\left[\nu^{(j)}-\nu'^{(j)}\left(D^2-k^2\right)\right]\right\}Dw^{(j)}=-k^2p_1^{(j)} \tag{17}$$

Eliminating the perturbed pressure $p_1^{(j)}$ between eqs. (15) and (17), we obtain

$$\left(D^2-k^2\right)\left(D^2-s_j^2\right)w^{(j)}=0 \tag{18}$$

where

$$s_j=\sqrt{k^2+\frac{ik_1^{(j)}\left(\varepsilon n+k_xU^{(j)}\right)+\varepsilon^2\nu^{(j)}}{\varepsilon^2\nu'^{(j)}}} \tag{19}$$

Also, the total electric fields in the two regions can be expressed in the forms

$$\boldsymbol{E}^{(j)}=-\frac{\partial\Psi_1^{(j)}}{\partial x}\boldsymbol{e_x}-\frac{\partial\Psi_1^{(j)}}{\partial y}\boldsymbol{e_y}-\left(E_0^{(j)}+\frac{\partial\Psi_1^{(j)}}{\partial z}\right)\boldsymbol{e_z} \tag{20}$$

where $\boldsymbol{e_x},\boldsymbol{e_y},\boldsymbol{e_z}$ are the unit vectors in the x,y,z directions, respectively.

Let the surface of elevation from the equilibrium state be defined as [34]

$$\xi=\delta\exp\left[i\left(k_xx+k_yy+nt\right)\right] \tag{21}$$

where δ is a small parameter. Also the unit normal vector $\boldsymbol{N}=\nabla F/|\nabla F|$ to the interface $F=z-\xi$ between the two fluids is defined, to the first order terms, in the form

$$\boldsymbol{N}=-ik_x\xi\boldsymbol{e_x}-ik_y\xi\boldsymbol{e_y}+\boldsymbol{e_z} \tag{22}$$

3. Boundary conditions and solutions

The solutions of eqs. (16) and (18) for both lower and upper fluid regions, respectively, can be expressed as

$$\Psi_1^{(j)}=A_j\exp\left[i\left(k_xx+k_yy+nt\right)\pm kz\right],\quad j=1,2 \tag{23}$$

$$\mathrm{w}^{(j)}=\left[B_j\exp(\pm kz)+C_j\exp\left(\pm s_jz\right)\right]\exp\left[i\left(k_xx+k_yy+nt\right)\right] \tag{24}$$

where A_j,B_j, and $C_j,(j=1,2)$, are the constants of integration to be determined using the following boundary conditions:

(1) The kinematic boundary condition in the two region should be satisfied at the interface, i.e.

$$\mathrm{w}^{(j)}=\varepsilon\frac{\partial\xi}{\partial t}+U^{(j)}\frac{\partial\xi}{\partial x} \quad \text{at} \quad z=0 \tag{25}$$

(2) The derivative of normal velocity components is continuous at the interface, i.e.

$$\mathrm{Dw}^{(1)}=\mathrm{Dw}^{(2)} \quad \text{at} \quad z=0 \tag{26}$$

Using eqs. (21) and (24) in the conditions (25) and (26), we obtain

$$B_1+C_1=i\left(\varepsilon n+k_xU^{(1)}\right)\delta \tag{27}$$

$$B_2+C_2=i\left(\varepsilon n+k_xU^{(2)}\right)\delta \tag{28}$$

$$kB_1+s_1C_1+kB_2+s_2C_2=0 \tag{29}$$

(3) Since the constitutive equations for the couple stress fluids in both regions are defined as

$$\tau_{ik} = \left(\mu - \mu'\nabla^2\right)\left(\frac{\partial v_i}{\partial x_k} + \frac{\partial v_k}{\partial x_i}\right) \tag{30}$$

Then, the tangential component of the stress tensor $\left(ik_x\tau_{xz} + ik_y\tau_{yz}\right)$ must continuous at the interface $z = \xi$, which yields with the help of eq. (12) to the following condition [3]

$$\left[\mu^{(1)} - \mu'^{(1)}\left(D^2 - k^2\right)\right]\left(D^2 + k^2\right)w^{(1)} = \left[\mu^{(2)} - \mu'^{(2)}\left(D^2 - k^2\right)\right]\left(D^2 + k^2\right)w^{(2)} \quad \text{at} \quad z = 0$$

Substitute for $w^{(1)}$ and $w^{(2)}$ from eqs. (24) into the last condition, we get

$$\begin{aligned}\left(2k^2\mu^{(1)}\right)B_1 + \left\{\left[\mu^{(1)} - \mu'^{(1)}\left(s_1^2 - k^2\right)\right]\left(s_1^2 + k^2\right)\right\}C_1 - \left(2k^2\mu^{(2)}\right)B_2 \\ - \left\{\left[\mu^{(2)} - \mu'^{(2)}\left(s_2^2 - k^2\right)\right]\left(s_2^2 + k^2\right)\right\}C_2 = 0 \quad \text{at} \quad z = 0\end{aligned} \tag{31}$$

Solving eqs. (27)-(29) and (31), we obtain

$$\begin{aligned}B_1 = i\delta\Big\{(s_1 - k)(s_2 + k)\left[\mu^{(2)} - \mu'^{(2)}\left(s_2^2 + k^2\right)\right] + \left(s_1^2 - k^2\right)\left[\mu^{(1)} - \mu'^{(1)}\left(s_1^2 + k^2\right)\right]\Big\}^{-1} \\ \times \Big\{(s_2 + k)\left[s_1\left(\varepsilon n + k_x U^{(1)}\right) + k\left(\varepsilon n + k_x U^{(2)}\right)\right]\left[\mu^{(2)} - \mu'^{(2)}\left(s_2^2 + k^2\right)\right] \\ + \left(s_1^2 + k^2\right)\left(\varepsilon n + k_x U^{(1)}\right)\left[\mu^{(1)} - \mu'^{(1)}\left(s_1^2 + k^2\right)\right] \\ + 2k^2\mu^{(2)}\left(\varepsilon n + k_x U^{(2)}\right)\Big\}\end{aligned} \tag{32}$$

$$\begin{aligned}C_1 = -i\delta\Big\{(s_1 - k)(s_2 + k)\left[\mu^{(2)} - \mu'^{(2)}\left(s_2^2 + k^2\right)\right] + \left(s_1^2 - k^2\right)\left[\mu^{(1)} - \mu'^{(1)}\left(s_1^2 + k^2\right)\right]\Big\}^{-1} \\ \times \Big\{(s_2 + k)\left[k\left(\varepsilon n + k_x U^{(1)}\right) + k\left(\varepsilon n + k_x U^{(2)}\right)\right]\left[\mu^{(2)} - \mu'^{(2)}\left(s_2^2 + k^2\right)\right] \\ + 2k^2\left[\mu^{(1)}\left(\varepsilon n + k_x U^{(1)}\right) + \mu^{(2)}\left(\varepsilon n + k_x U^{(2)}\right)\right]\Big\}\end{aligned} \tag{33}$$

$$\begin{aligned}B_2 = i\delta\Big\{\left(s_2^2 - k^2\right)\left[\mu^{(2)} - \mu'^{(2)}\left(s_2^2 + k^2\right)\right] + (s_2 - k)(s_1 + k)\left[\mu^{(1)} - \mu'^{(1)}\left(s_1^2 + k^2\right)\right]\Big\}^{-1} \\ \times \Big\{\left(s_2^2 - k^2\right)\left(\varepsilon n + k_x U^{(2)}\right)\left[\mu^{(2)} - \mu'^{(2)}\left(s_2^2 + k^2\right)\right] \\ + (s_1 + k)\left[s_2\left(\varepsilon n + k_x U^{(2)}\right) + k\left(\varepsilon n + k_x U^{(1)}\right)\right]\left[\mu^{(1)} - \mu'^{(1)}\left(s_1^2 + k^2\right)\right] \\ - 2k^2\left[\mu^{(1)}\left(\varepsilon n + k_x U^{(1)}\right) + \mu^{(2)}\left(\varepsilon n + k_x U^{(2)}\right)\right]\Big\}\end{aligned} \tag{34}$$

$$\begin{aligned}C_2 = -i\delta\Big\{\left(s_2^2 - k^2\right)\left[\mu^{(2)} - \mu'^{(2)}\left(s_2^2 + k^2\right)\right] + (s_2 - k)(s_1 + k)\left[\mu^{(1)} - \mu'^{(1)}\left(s_1^2 + k^2\right)\right]\Big\}^{-1} \\ \times \Big\{(s_1 + k)\left[k\left(\varepsilon n + k_x U^{(1)}\right) + k\left(\varepsilon n + k_x U^{(2)}\right)\right]\left[\mu^{(1)} - \mu'^{(1)}\left(s_1^2 + k^2\right)\right] \\ - 2k^2\left[\mu^{(1)}\left(\varepsilon n + k_x U^{(1)}\right) + \mu^{(2)}\left(\varepsilon n + k_x U^{(2)}\right)\right]\Big\}\end{aligned} \tag{35}$$

(4) The tangential component of the electric field is continuous at the interface, i.e.

$$\boldsymbol{N} \times \boldsymbol{E}^{(1)} = \boldsymbol{N} \times \boldsymbol{E}^{(2)} \quad \text{at} \quad z = 0 \tag{36}$$

Substitute from eqs. (20) and (22) into the condition (36), then to the first order terms, we obtain

$$\frac{\partial \Psi_1^{(1)}}{\partial y} - \frac{\partial \Psi_1^{(1)}}{\partial y} = ik_y\xi\left(E_0^{(2)} - E_0^{(1)}\right) \tag{37}$$

(5) The normal component of the electric displacement is continuous at the interface, i.e.

$$\boldsymbol{N}\cdot\left(\epsilon^{(1)}\boldsymbol{E}^{(1)}\right)=\boldsymbol{N}\cdot\left(\epsilon^{(1)}\boldsymbol{E}^{(1)}\right)\quad\text{at}\quad z=0 \tag{38}$$

Then, to the first order terms, we obtain

$$\epsilon^{(1)}\frac{\partial\Psi_1^{(1)}}{\partial z}-\epsilon^{(2)}\frac{\partial\Psi_1^{(2)}}{\partial z}=0\quad\text{at}\quad z=0 \tag{39}$$

Using eq. (23), then eqs. (37) and (39), yield

$$A_1-A_2=\delta\left(E_0^{(2)}-E_0^{(1)}\right) \tag{40}$$

$$\epsilon^{(1)}A_1+\epsilon^{(2)}A_2=0 \tag{41}$$

Solving eqs. (40) and (41), we obtain

$$A_j=\pm\frac{\delta\epsilon^{(j\pm1)}\left(E_0^{(2)}-E_0^{(1)}\right)}{\left(\epsilon^{(1)}+\epsilon^{(2)}\right)} \tag{42}$$

Since, there are no surface charges present at the interface, then the following condition $\epsilon^{(1)}E_0^{(1)}=\epsilon^{(2)}E_0^{(2)}$ should be satisfied, then in this case eq. (42) reduces to [35]

$$A_j=\mp\frac{\delta E_0^{(j)}\left(\epsilon^{(2)}-\epsilon^{(1)}\right)}{\left(\epsilon^{(1)}+\epsilon^{(2)}\right)} \tag{43}$$

From eqs. (23) and (43), we obtain the following solution

$$\Psi_1^{(j)}=\mp\frac{E_0^{(j)}\left(\epsilon^{(2)}-\epsilon^{(1)}\right)\xi}{\left(\epsilon^{(1)}+\epsilon^{(2)}\right)}\exp(\pm kz) \tag{44}$$

(6) The normal component of the stress tensor should be discontinuous at the interface by the surface tension coefficient T, then to the first order terms, we obtain the following condition [25]

$$\xi\left[\frac{\partial p_0^{(1)}}{\partial z}-\frac{\partial p_0^{(2)}}{\partial z}\right]+p_1^{(1)}-p_1^{(2)}+\epsilon^{(2)}E_0^{(2)}\frac{\partial\Psi_1^{(2)}}{\partial z}-\epsilon^{(1)}E_0^{(1)}\frac{\partial\Psi_1^{(1)}}{\partial z}=-T\nabla^2\xi\quad\text{at}\quad z=0 \tag{45}$$

From eqs. (17) and (24), we can write the pressure in the region $z<0$, in the form

$$p_1^{(1)}=-\frac{\rho^{(1)}}{k^2}\left\{\left[\frac{i}{\varepsilon^2}\left(\varepsilon n+k_xU^{(1)}\right)+\frac{\nu^{(1)}}{k_1^{(1)}}\right]\left[B_1k\exp(kz)+C_1s_1\exp(s_1z)\right]\right.$$
$$\left.-\frac{\nu'^{(1)}}{k_1^{(1)}}s_1\left(s_1^2-k^2\right)C_1\exp(s_1z)\right\}\exp\left[i\left(k_xx+k_yy+nt\right)\right] \tag{46}$$

and in the region $z>0$, it takes the form

$$p_1^{(2)}=\frac{\rho^{(2)}}{k^2}\left\{\left[\frac{i}{\varepsilon^2}\left(\varepsilon n+k_xU^{(2)}\right)+\frac{\nu^{(2)}}{k_1^{(2)}}\right]\left[B_2k\exp(-kz)+C_2s_2\exp(-s_2z)\right]\right.$$
$$\left.-\frac{\nu'^{(2)}}{k_1^{(2)}}s_2\left(s_2^2-k^2\right)C_2\exp(-s_2z)\right\}\exp\left[i\left(k_xx+k_yy+nt\right)\right] \tag{47}$$

Also, from eq. (1), we have to the zero order terms, in the two regions, the following equation

$$\frac{\partial p_0^{(j)}}{\partial z}=-\rho^{(j)}g \tag{48}$$

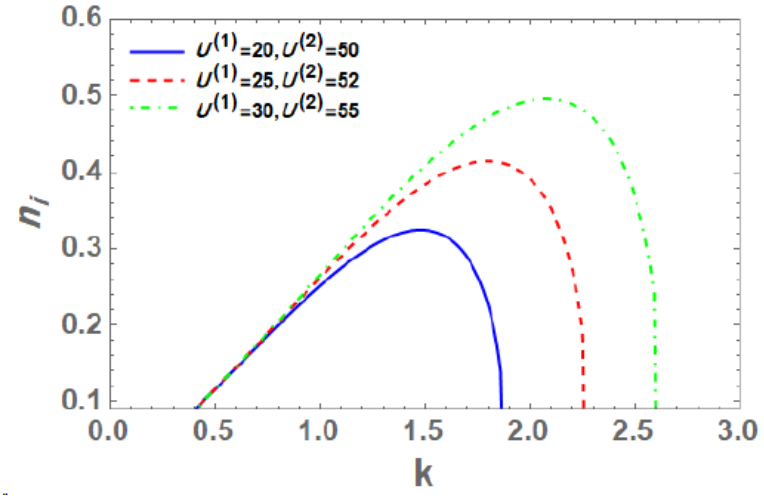

Fig. 1. Variation of the negative imaginary part of growth rate versus the wave number for various values of fluid velocities $U^{(1)}$ and $U^{(2)}$ in asystem having:$V^{(1)} = 0.5\ cm^2/s$, $V^{(2)} = 0.2\ cm^2/s$, $V'^{(1)} = 0.5\ cm^4/s$, $V'^{(2)} = 0.2\ cm^4/s$, $k_1^{(1)} = 20\ cm^2$, $k_1^{(2)} = 30\ cm^2$, $\epsilon^{(1)} = 0.3$, $\epsilon^{(2)} = 0.1$, $E_0^{(1)} = 100$ stat$V$/cm, $E_0^{(2)} = 50$ stat$V$/cm, $\rho^{(1)} = 10\ gr/cm^3$, $\rho^{(2)} = 5\ gr/cm^3$, $g = 980\ cm/s^2$, $T = 72\ dyn/cm$, $\varepsilon = 1$.

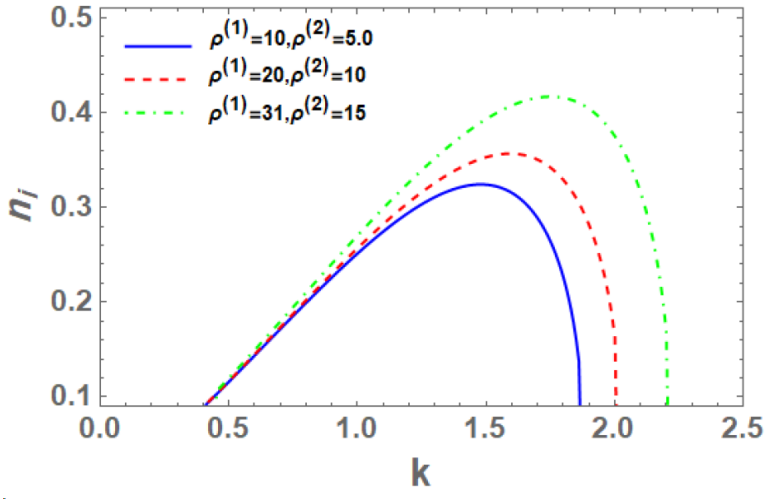

Fig. 2. Variation of the negative imaginary part of growth rate versus the wave number for various values of fluid densities $\rho^{(1)}$ and $\rho^{(2)}$ in a system having: $U^{(1)} = 20\ cm/s$, $U^{(2)} = 50\ cm/s$,$V^{(1)} = 0.5\ cm^2/s$, $V^{(2)} = 0.2\ cm^2/s$ $V'^{(1)} = 0.5\ cm^4/s$, $V'^{(2)} = 0.2\ cm^4/s$, $k_1^{(1)} = 20\ cm^2$, $k_1^{(2)} = 30\ cm^2$, $\epsilon^{(1)} = 0.3$, $\epsilon^{(2)} = 0.1$, $E_0^{(1)} = 100$ stat$V$/cm, $E_0^{(2)} = 50$ stat$V$/cm, $g = 980\ cm/s^2$, $T = 72\ dyn/cm$, $\varepsilon = 1$.

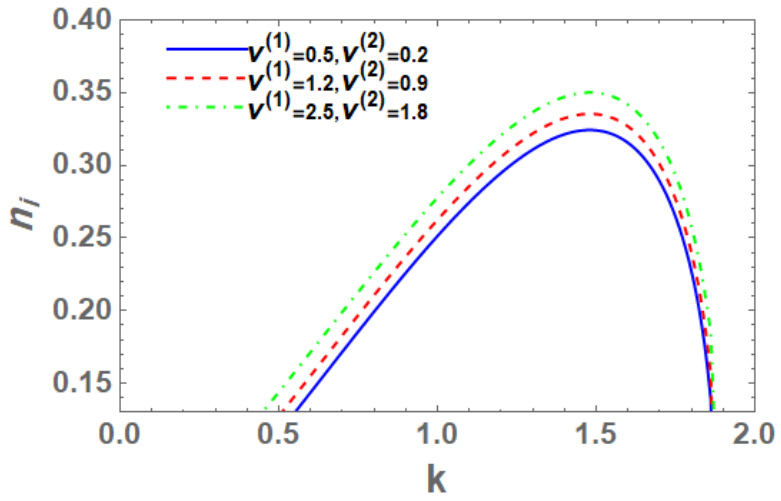

Fig. 3. Variation of the negative imaginary part of growth rate versus the wave number for various values of kinematic viscosities $V^{(1)}$ and $V^{(2)}$ in a system having: $U^{(1)} = 20\ cm/s$, $U^{(2)} = 50\ cm/s$, $V'^{(1)} = 0.5\ cm^4/s$, $V'^{(2)} = 0.2\ cm^4/s$, $k_1^{(1)} = 20\ cm^2$, $k_1^{(2)} = 30\ cm^2$, $\epsilon^{(1)} = 0.3$, $\epsilon^{(2)} = 0.1$, $E_0^{(1)} = 100$ stat$V$/cm, $E_0^{(2)} = 50$ stat$V$/cm,$\rho^{(1)} = 10\ gr/cm^3$, $\rho^{(2)} = 5\ gr/cm^3$ $g = 980\ cm/s^2$, $T = 72\ dyn/cm$, $\varepsilon = 1$.

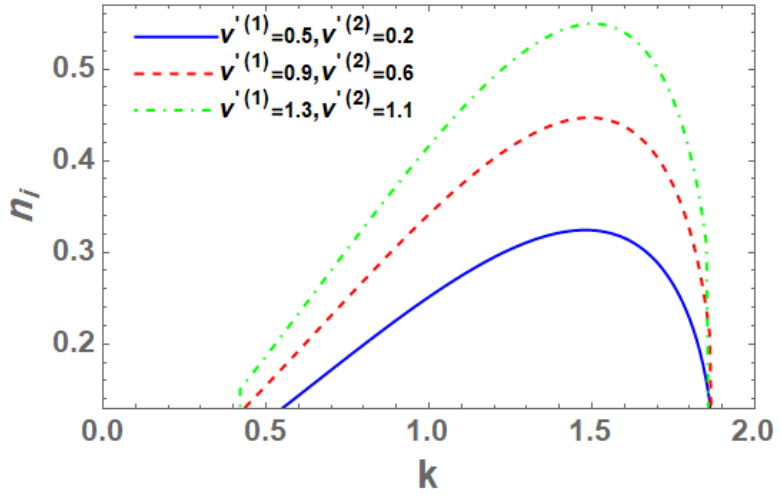

Fig. 4. Variation of the negative imaginary part of growth rate versus the wave number for various values of kinematic viscoelasticity $v'^{(1)}$ and $v'^{(2)}$ in a system having: $U^{(1)} = 20\ cm/s$, $U^{(2)} = 50\ cm/s$, $V^{(1)} = 0.5\ cm^2/s$, $V^{(2)} = 0.2\ cm^2/s$, $k_1^{(1)} = 20\ cm^2$, $k_1^{(2)} = 30\ cm^2$, $\epsilon^{(1)} = 0.3$, $\epsilon^{(2)} = 0.1$, $E_0^{(1)} = 100$ stat$V$/cm, $E_0^{(2)} = 50$ stat$V$/cm, $\rho^{(1)} = 10\ gr/cm^3$, $\rho^{(2)} = 5\ gr/cm^3$, $g = 980\ cm/s^2$, $T = 72\ dyn/cm$, $\varepsilon = 1$.

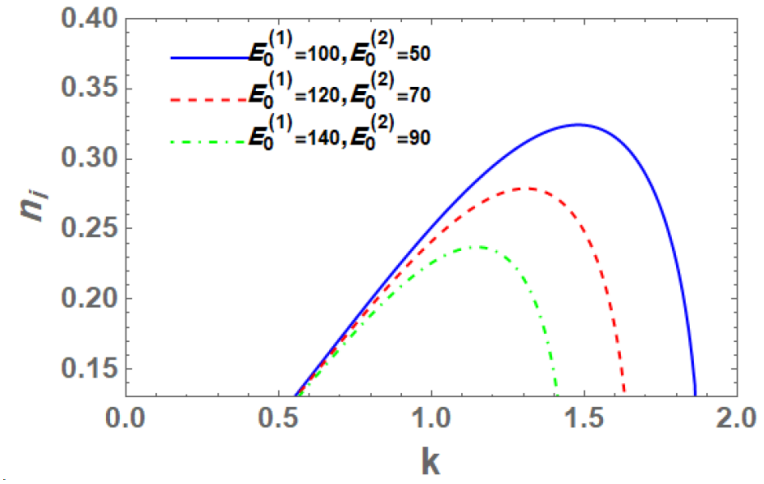

Fig. 5. Plot of variation of the negative imaginary part of growth rate versus the wave number for various values of electric fields $E_0^{(1)}$ and $E_0^{(2)}$ in a system having: $U^{(1)} = 20\ cm/s$, $U^{(2)} = 50\ cm/s$, $V^{(1)} = 0.5\ cm^2/s$, $V^{(2)} = 0.2\ cm^2/s$ $V'^{(1)} = 0.5\ cm^4/s$, $V'^{(2)} = 0.2\ cm^4/s$, $k_1^{(1)} = 20\ cm^2$, $k_1^{(2)} = 30\ cm^2$,$\epsilon^{(1)} = 0.3$, $\epsilon^{(2)} = 0.1$,$\rho^{(1)} = 10\ gr/cm^3$, $\rho^{(2)} = 5\ gr/cm^3$ $g = 980\ cm/s^2$, $T = 72\ dyn/cm$, $\varepsilon = 1$.

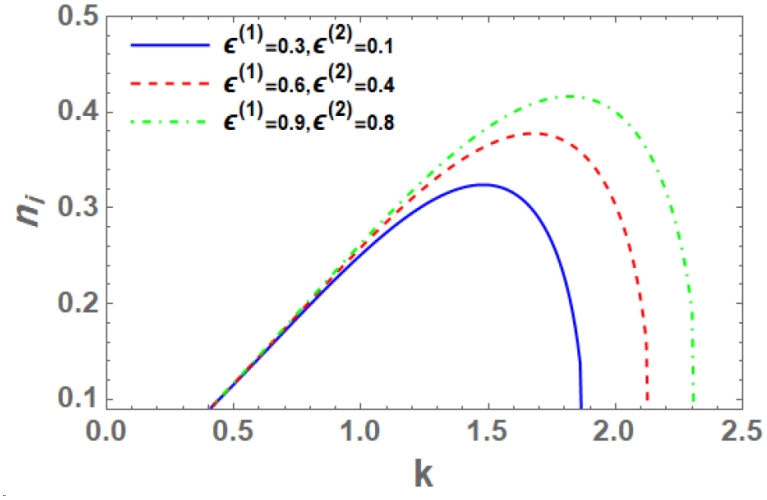

Fig. 6. Plot of variation of the negative imaginary part of growth rate versus the wave number for various values of dielectric constants $\epsilon^{(1)}$ and $\epsilon^{(1)}$ in a system having: $U^{(1)} = 20\ cm/s$, $U^{(2)} = 50\ cm/s$, $V^{(1)} = 0.5\ cm^2/s$, $V^{(2)} = 0.2\ cm^2/s$ $V'^{(1)} = 0.5\ cm^4/s$, $V'^{(2)} = 0.2\ cm^4/s$, $k_1^{(1)} = 20\ cm^2$, $k_1^{(2)} = 30\ cm^2$, $E_0^{(1)} = 100$ stat$V$/cm, $E_0^{(2)} = 50$ stat$V$/cm,$\rho^{(1)} = 10\ gr/cm^3$, $\rho^{(2)} = 5\ gr/cm^3$ $g = 980\ cm/s^2$, $T = 72\ dyn/cm$, $\varepsilon = 1$.

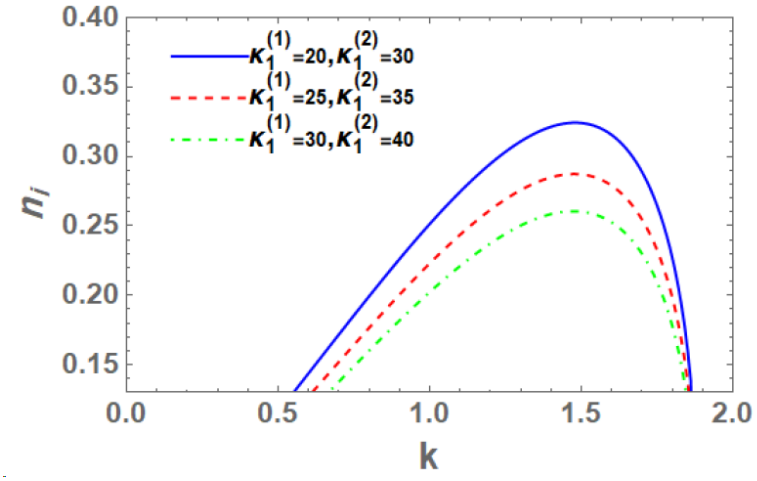

Fig. 7. Plot of variation of the negative imaginary part of growth rate versus the wave number for various values of medium permeabilities $k_1^{(1)}$ and $k_1^{(2)}$ in a system having: $U^{(1)} = 20\ cm/s$, $U^{(2)} = 50\ cm/s$, $V^{(1)} = 0.5\ cm^2/s$, $V^{(2)} = 0.2\ cm^2/s$ $V'^{(1)} = 0.5\ cm^4/s$, $V'^{(2)} = 0.2\ cm^4/s$,$\epsilon^{(1)} = 0.3$, $\epsilon^{(2)} = 0.1$ $E_0^{(1)} = 100$ stat$V$/cm, $E_0^{(2)} = 50$ stat$V$/cm,$\rho^{(1)} = 10\ gr/cm^3$, $\rho^{(2)} = 5\ gr/cm^3$ $g = 980\ cm/s^2$, $T = 72\ dyn/cm$, $\varepsilon = 1$.

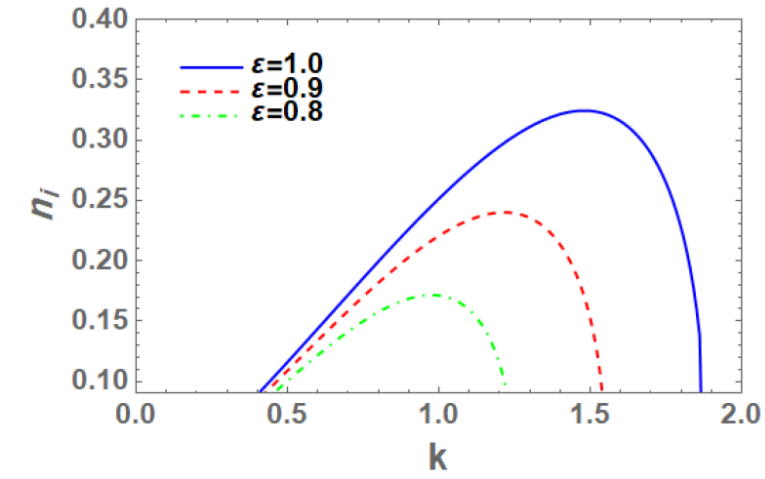

Fig. 8. Plot of variation of the negative imaginary part of growth rate versus the wave number for various values of porosity of the porous medium ε in a system having: $U^{(1)} = 20\ cm/s$, $U^{(2)} = 50\ cm/s$, $V^{(1)} = 0.5\ cm^2/s$, $V^{(2)} = 0.2\ cm^2/s$ $V'^{(1)} = 0.5\ cm^4/s$, $V'^{(2)} = 0.2\ cm^4/s$,$k_1^{(1)} = 20\ cm^2$, $k_1^{(2)} = 30\ cm^2$,$\epsilon^{(1)} = 0.3$, $\epsilon^{(2)} = 0.1$ $E_0^{(1)} = 100$ stat$V$/cm, $E_0^{(2)} = 50$ stat$V$/cm,$\rho^{(1)} = 10\ gr/cm^3$, $\rho^{(2)} = 5\ gr/cm^3$ $g = 980\ cm/s^2$, $T = 72\ dyn/cm$

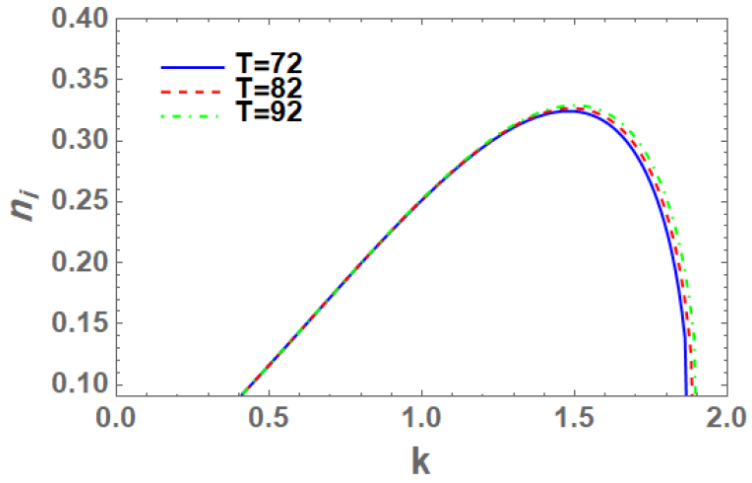

Fig. 9. Plot of variation of the negative imaginary part of growth rate versus the wave number for various values of surface tension T in a system having: $U^{(1)} = 20\ cm/s$, $U^{(2)} = 50\ cm/s$, $V^{(1)} = 0.5\ cm^2/s$, $V^{(2)} = 0.2\ cm^2/s$ $V'^{(1)} = 0.5\ cm^4/s$, $V'^{(2)} = 0.2\ cm^4/s$,$k_1^{(1)} = 20\ cm^2$, $k_1^{(2)} = 30\ cm^2$,$\epsilon^{(1)} = 0.3$, $\epsilon^{(2)} = 0.1$ $E_0^{(1)} = 100$ stat$V$/cm, $E_0^{(2)} = 50$ stat$V$/cm,$\rho^{(1)} = 10\ gr/cm^3$, $\rho^{(2)} = 5\ gr/cm^3$ $g = 980\ cm/s^2$, $\varepsilon = 1$.

4. Dispersion relation and stability analysis

Substitute from eqs. (21), (23), (44), (46)-(49) into the normal stress boundary condition (45), we obtain the following dispersion relation

$$
\begin{aligned}
&\left[gk\left(\rho^{(1)}-\rho^{(2)}\right)+Tk^3-\frac{k^2E_0^{(1)}E_0^{(2)}\left(\epsilon^{(2)}-\epsilon^{(1)}\right)^2}{\left(\epsilon^{(1)}+\epsilon^{(2)}\right)}\right]\\
&\times\left\{\rho^{(2)}\left(s_1-k\right)\left(s_2+k\right)\left[\nu^{(2)}-\nu'^{(2)}\left(s_2^2+k^2\right)\right]+\rho^{(1)}\left(s_1^2-k^2\right)\left[\nu^{(1)}-\nu^{(1)}\left(s_1^2+k^2\right)\right]\right\}\\
&\times\left\{\rho^{(2)}\left(s_2^2-k^2\right)\left[\nu^{(2)}-\nu^{(2)}\left(s_2^2+k^2\right)\right]+\rho^{(1)}\left(s_2-k\right)\left(s_1+k\right)\left[\nu^{(1)}-\nu'^{(1)}\left(s_1^2+k^2\right)\right]\right\}\\
&+i\rho^{(1)}\left\{\rho^{(2)}\left(s_2^2-k^2\right)\left[\nu^{(2)}-\nu'^{(2)}\left(s_2^2+k^2\right)\right]+\rho^{(1)}\left(s_2-k\right)\left(s_1+k\right)\right.\\
&\left.\times\left[\nu^{(1)}-\nu'^{(1)}\left(s_1^2+k^2\right)\right]\right\}\left\{\left[\frac{i}{\varepsilon^2}\left(\varepsilon n+k_xU^{(1)}\right)+\frac{\nu^{(1)}}{k_1^{(1)}}\right]\right.\\
&\times\left\{-\rho^{(2)}\left(s_1-k\right)\left(s_2+k\right)\left(\varepsilon n+k_xU^{(2)}\right)\left[\nu^{(2)}-\nu'^{(2)}\left(s_2^2+k^2\right)\right]+\rho^{(1)}\left(\varepsilon n+k_xU^{(1)}\right)\right.\\
&\left.\left.\times\left[\nu^{(1)}-\nu'^{(1)}\left(s_1^2+k^2\right)\right]-2k\rho^{(2)}\nu^{(2)}\left(s_1-k\right)\left(\varepsilon n+k_xU^{(2)}\right)\right\}\right.\\
&+\frac{\nu'^{(1)}}{k_1^{(1)}}s_1\left(s_1^2-k^2\right)\left\{\rho^{(2)}\left[\left(\varepsilon n+k_xU^{(1)}\right)+\left(\varepsilon n+k_xU^{(2)}\right)\right]\right.\\
&\left.\left.\times\left[\nu^{(2)}-\nu'^{(2)}\left(s_2^2+k^2\right)\right]+2k\left[\rho^{(1)}\nu^{(1)}\left(\varepsilon n+k_xU^{(1)}\right)+\rho^{(2)}\nu^{(2)}\left(\varepsilon n+k_xU^{(2)}\right)\right]\right\}\right\}\\
&+i\rho^{(2)}\left\{\rho^{(2)}\left(s_1-k\right)\left(s_2+k\right)\left[\nu^{(2)}-\nu'^{(2)}\left(s_2^2+k^2\right)\right]\right.\\
&\left.+\rho^{(1)}\left(s_1^2-k^2\right)\left[\nu^{(1)}-\nu'^{(1)}\left(s_1^2+k^2\right)\right]\right\}\left\{\left[\frac{i}{\varepsilon^2}\left(\varepsilon n+k_xU^{(2)}\right)+\frac{\nu^{(2)}}{k_1^{(2)}}\right]\right.\\
&\times\left\{\rho^{(2)}\left(s_2^2-k^2\right)\left(\varepsilon n+k_xU^{(2)}\right)\left[\nu^{(2)}-\nu'^{(2)}\left(s_2^2+k^2\right)\right]\right.\\
&-\rho^{(1)}\left(s_1+k\right)\left(s_2-k\right)\left(\varepsilon n+k_xU^{(1)}\right)\left[\nu^{(1)}-\nu'^{(1)}\left(s_1^2+k^2\right)\right]\\
&\left.+2k\left(s_2-k\right)\left[\rho^{(1)}\nu^{(1)}\left(\varepsilon n+k_xU^{(1)}\right)+\rho^{(2)}\nu^{(2)}\left(\varepsilon n+k_xU^{(2)}\right)\right]\right\}+\frac{\nu'^{(2)}}{k_1^{(2)}}s_2\left(s_2^2-k^2\right)\\
&\times\left\{\rho^{(1)}\left(s_1+k\right)\left[\left(\varepsilon n+k_xU^{(1)}\right)+\left(\varepsilon n+k_xU^{(2)}\right)\right]\left[\nu^{(1)}-\nu'^{(1)}\left(s_1^2+k^2\right)\right]\right.\\
&\left.\left.-2k\left[\rho^{(1)}\nu^{(1)}\left(\varepsilon n+k_xU^{(1)}\right)+\rho^{(2)}\nu^{(2)}\left(\varepsilon n+k_xU^{(2)}\right)\right]\right\}\right\}=0
\end{aligned}
\tag{49}
$$

In the linear temporal stability analysis, considered here, the instability of the interface between two fluids occurs in light of the negative values of the growth rate disturbance (i.e., $n_i \leq 0$). This growth rate disturbance between the two media can be gained by solving the corresponding dispersion relation. Since the dimensional dispersion relation as given in eq. (49) is rather complicated. Actually, its analytical solution, in a closed-form, cannot be determined. Therefore, using the Mathematica software, a similar procedure, as given previously by El-Sayed et al. [36]-[38], a numerical technique has been applied. For this purpose, in view of the Gaster [33] theorem, setting $n_r = -k$, taken into account that $n_i = 5$, say, as an initial guess for the root. An iteration of the solution as ordered pairs, for different values of the other physical parameters included in this investigation, is obtained. Therefore, one gets the required data, and consequently, the required graph can be plotted as the variation of negative imaginary part of the growth rate n_i with the wavenumber k for various values of the other physical parameters including in the analysis as shown in Figs. (1)-(9) . The maximum growth rates, in these figures, and the related wave numbers are both referred to as the dominant growth rates and the dominant wave numbers. The critical wave number k_c is the point where the growth rate curve intersects the wave number axis and it is called the cutoff wave number. The region under the growth rate curve in these figures is called the instability zone.

Figure 1 shows the variation of the negative imaginary part of growth rate n_i versus the wave number k for different values of the fluid velocities $U^{(1)}$ and $U^{(2)}$, and constant values of the other physical parameters. This graph clearly shows that when the fluid velocities $U^{(1)}$ and $U^{(2)}$ rise, so do the dominant growth rates, dominant wave numbers, and critical wave numbers since all growth rate curves have the same starting wave number. Consequently, the instability zone expands, demonstrating that the velocities $U^{(1)}$ and $U^{(2)}$ of couple stress fluids destabilize the system.

Figure 2 shows the relationship between the negative imaginary part of growth rate n_i and the wave number k for various fluid densities $\rho^{(1)}$ and $\rho^{(2)}$ values, and constant other physical parameters. Increasing the fluid densities $\rho^{(1)}$ and $\rho^{(2)}$ values, increase also each of the maximum dominant growth rates, dominant wave numbers, and critical wave numbers such that the starting point remains constant. Hence, we conclude that the fluid densities $\rho^{(1)}$ and $\rho^{(2)}$ have destabilizing effects also because they increase the instability zones.

Figure 3 shows how the negative imaginary part of growth rate n_i changes with the wave number k for under various values of the kinematics viscosities $\upsilon^{(1)}$ and $\upsilon^{(2)}$ of couple stress fluids, and constant values of the other physical parameters. We see in this figure that as the kinematics viscosities $\upsilon^{(1)}$ and $\upsilon^{(2)}$ are increased, dominant and critical wave numbers remain at predetermined values due to lower maximum dominant growth rates. Increased values of kinematics viscosities $\upsilon^{(1)}$ and $\upsilon^{(2)}$ of couple stress fluids has destabilizing effects in the system of interest since the instability zone increases.

Figure 4 depicts the variation of the negative imaginary part of growth rate n_i versus the wave number k for different values of the kinematics viscoelasticities $\upsilon'^{(1)}$ and $\upsilon'^{(2)}$ of couple stress electrified fluids,and constant values of the other physical parameters. Increasing the kinematics viscoelasticities $\upsilon'^{(1)}$ and $\upsilon'^{(2)}$ decrease the maximum dominant growth rates, but they remain at the same dominant wave number value. As a result, we may deduce that increasing the kinematics viscoelasticities $\upsilon'^{(1)}$ and $\upsilon'^{(2)}$ of couple stress fluids stabilize this system by raising the starting wave numbers and keep critical wave numbers, while decreasing the instability zone.

Figure 5 shows the variation of the negative imaginary part of growth rate n_i versus the wave number k for different values of the normal electric fields $E_0^{(1)}$ and $E_0^{(2)}$ and constant values of the other physical parameters. It can be seen from the figure that the maximum dominant growth rates as well as the dominant and critical wave numbers decrease by increasing the normal electric fields values, while all the growth rate curves have the same starting wave number value. Hence, the instability zone shrinks when the electric fields values are increased, indicating that the normal electric fields $E_0^{(1)}$ and $E_0^{(2)}$ have stabilizing effect on the system of couple stress fluids in presence of porous media.

Figure 6 shows the variation of the negative imaginary part of growth rate n_i versus the wave number k under several different values of the dielectric constants $\epsilon^{(1)}$ and $\epsilon^{(2)}$ and constant values of the other physical parameters. It can clear from this figure that the maximum dominant growth rates as well as the dominant and critical wave numbers increase by increasing the dielectric constants values, while all the growth rate curves have the same starting wave number value. Hence, the instability zone expands when the dielectric constants values are increased, demonstrating that the dielectric constants $\epsilon^{(1)}$ and $\epsilon^{(2)}$ have destabilizing effect on this system of couple stress fluids in presence of porous media.

Figure 7 shows the effects of medium permeabilities of porous media $k_1^{(1)}$ and $k_1^{(2)}$ on the negative imaginary part of growth rate n_i and the wave number k, and the other parameters stay constants. From this figure, it is clear that when the medium permeabilities of porous media are increased, both the maximum dominant growth rates and the dominant wave numbers decrease, while the critical wave numbers remains the same such that the instability zone shrinks in this case. Therefore, we conclude that medium permeabilities of porous media $k_1^{(1)}$ and $k_1^{(2)}$ have stabilizing effects on the system under consideration of electrified couple stress viscoelastic fluids.

Figure 8 demonstrates the variation of the negative imaginary part of growth rate n_i versus the wave number k for different values of the porosity of porous medium ε and constant values of the other parameters. It is obvious from this figure that the maximum dominant growth rate, dominant wave numbers and the critical wave numbers values decrease, while the starting wave numbers values increase due increasing of the porosity of porous medium, and this lead to reduce the instability zone. Then, we conclude that the porosity of porous medium ε has a stabilizing influence on the system.

Figure 9 shows the negative imaginary part of growth rate n_i in relation to the wave number k for different values of surface tension T with constant values of the other parameters. As the surface tension value is increased, the resultant curves are gradually increase slightly after a fixed wave number value greater than one as seen by the curves behavior. The surface tension T has a small destabilizing influence on the system under consideration, therefore we can draw this conclusion.

5. Concluding remarks

The linear analysis of the Kelvin-Helmholtz instability of two superposed semi-infinite dielectric viscoelastic fluids of couple stress type in the presence of porous media with various medium permeabilities and electric fields has been explored in this article. In order to express the growth rates in terms of wave numbers for constant values of the other physical parameters included in the study, we use perturbations and normal modes methodologies for the governing equations of motion and boundary conditions for coupled stress fluids and electric fields. As a result of Gaster's iterative process, the derived dispersion relation was numerically solved in Mathematica to yield growth rates through a guess value. As shown in the following graphs, a variety of parameters have an impact on the stability of the system under consideration.

(1) There is a stabilizing influence on the considered system for each of fluid velocity, fluid kinematic viscosity, fluid density, and dielectric constant.

(2) The system is destabilized by the fluid kinematic viscoelasticities, medium permeabilities, porous medium porosity, and electrical fields.

(3) The Kelvin-Helmholtz instability is suppressed by the surface tension in the presence of couple stress fluids and applied electric fields, according to this study.

References

[1] R. C. Sharma, Sunil, M. Pal, On superposed couple-stress fluid in porous medium, Studia Geotech. Mech. 33 (2001) 55-66.
[2] R. C. Sharma, Sunil, Y. D. Sharma, R. S. Chandel, On couple-stress fluid permeated with suspended particles heated from below, Arch. Mech. 54 (2002) 287-298.
[3] Sunil, R. C. Sharma. R. S. Chandel, On superposed couple-stress fluids in porous medium in hydromagnetics, Z, Naturforsch. A 57 (2002) 955-960.
[4] N. Rudraiah, B. M. Shankar, Stability of parallel couple stress viscous fluid flow in a channel, Int. J. Appl. Math. 1 (2009) 67-78.
[5] R. K. Naeem, A class of flows for couple stress fluids, J. Basic & Appl. Sci. 8 (2012) 97-104.
[6] V. K. Stokes, Couple stresses in fluids, Phys. Fluids 9 (1966) 1709-1715.
[7] V. K. Stokes, Effects of couple stress in fluid on hydromagnetic channel flow, Phys. Fluids 11, (1968) 1131-1133.
[8] K. B. Chavaraddi, V. B. Awati, P. M. Gouder, Effects of boundary roughness on Rayleigh-Taylor instability of a couple-stress fluid, Gen. Math. Notes 17 (2013) 66-75.
[9] K. B. Chavaraddi, N. N. Katagi, V. B. Awati, P. M. Gouder, Effect of boundary roughness on Kelvin-Helmholtz instability in couple stress fluid layer bounded above by a porous layer and below by rigid surface, Int. J. Chem. Eng. Res. 4 (2014) 35-43.
[10] V. B. Awati, K. B. Chavaraddi, P. M. Gouder, Effects of boundary roughness on nonlinear saturation of Rayleigh-Taylor instability in couple-stress fluid, Nonlinear Eng.: Model. & Appls. 8 (2019) 39-45.
[11] K. B. Chavaraddi, P. M. Gouder, R. B. Kudenatti, The influence of boundary roughness on Rayleigh-Taylor instability at the interface of superposed couple-stress fluids, J. Adv. Res. Fluid Mech. & Thermal Sci. 75 (2020) 1-10.
[12] P. Kumar, G. J. Sing, Analysis of stability in couple-stress magneto-fluid, Nepal J. Math. Sci., vol. 2 (2021) 35-42.
[13] U. Munivenkatappa, D. P. Aswathanarayana, A. S. Reddy, S. B. Ramakrishna, Effect of couple stress fluid in an irregular couette flow channel: An analytical approach, Biointerface Res. Appl. Chem. 12 (2022) 4686-4704.
[14] O. M. Phillips, Flow and Reaction in Permeable Rocks, Cambridge University Press, Cambridge, 1991.
[15] D. B. Ingham, I. Pop, Transport Phenomena in Porous Medium, Pergamon, Oxford, 1998.
[16] A. Bejan, Porous and Complex Flow Structure in Modern Technology, Springer, Berlin, 2004.
[17] B. Straughan, Stability and Wave Motion in Porous Media, Applied Mathematical Sciences, Springer-Verlag, New York, 2008.

[18] D. A. Nield, A. Bejan, Convection in Porous Medium,, 4th ed., Springer-Verlag, New York, 2013.
[19] R. Rudrauah, G. Chandrashekara, Effects of couple stress on the growth rate of Rayleigh-Taylor instability at the interface in a finite thickness couple stress fluid, J. Appl. Fluid Mech. 3 (2010) 83-89.
[20] R. P. Mathur, D. Gupta, Effect of surface tension on the stability of superposed viscous- viscoelastic (couple-stress) fluids through porous medium, Proc. Indian Nat. Sci. Acad., 77 (2011) 335-342.
[21] I. S Shivakumara, J. Lee, S. S. Kumar, N. Devaraja, N., Linear and nonlinear stability of double diffusive convection in a couple stress fluid- saturated porous layer, Arch. Appl. Mech. 81 (2011) 1697-1715.
[22] I. S Shivakumara, S. S., Kumar, N. Devaraja, Effect of non-uniform temperature gradients on the onset of convection in couple stress fluid- saturated porous medium, J. Appl. Fluid Mech. 5 (2012) 49- 55.
[23] M. B. Agoor, N. T. M. Eldabe, Rayleigh-Taylor instability at the interface of superposed couple- stress casson fluids flow in porous medium under the effect of a magnetic field, J. Appl. Fluid. Mech., 7 (2014) 573-580.
[24] B. M. Shankar, I. S Shivakumara, C.-O. Ng, Stability of couple stress fluid flow through a horizontal porous layer, J. Porous Med. 19 (2016) 391-404.
[25] J. R. Melcher, Continuum Electromechanics, MIT Press, Cambridge, MA, 1981.
[26] J. A. Del Rio, S. Whitaker, Electrohydrodynamics in Porous Media, Trans. Porous Med. 44 (2001) 385-405.
[27] N. Rudraiah, B. M. Shankar, C.-O. Ng, Electrohydrodynamic stability of couple stress fluid flow in a channel occupied by a porous medium, Special Topics & Rev. in Porous Med. 2 (2011) 11-22.
[28] I. S Shivakumara, M. Akkanagamma, M., C.-O. Ng, Electrohydrodynamic instability of a rotating couple-stress dielectric fluid layer, Int. J. Heat Mass Transf. 62 (2013) 761-771.
[29] B. M. Shankar, J. Kumar, I. S Shivakumara, Stability of natural convection in a vertical couple stress fluid layer in the presence of a horizontal AC electric field, Appl. Math. Model. 40 (2016) 5462- 5481.
[30] G. C. Rana, H. Saxena, P. K. Gautam, The onset of electrohydrodynamic instability in a couple- stress nanofluid saturating a porous medium: Brinkman model, Rev. Cubana Fis. 36 (2019) 37-45.
[31] M. F. El-Sayed, N. T. Eldabe, M. H. Haroun, D. M. Mastafa, Nonlinear electroviscous potential flow instability of two superposed couple-stress fluids streaming through porous medium, J. Porous Med. 17 (2014) 405-420.
[32] M. F. El-Sayed, A. M. Alanzi, Electrohydrodynamic liquid sheet instability of moving viscoelastic couple-stress dielectric fluid surrounded by an inviscid gas through porous medium, fluids (MDPI) 7 (2022), article 247 (23 pages).
[33] M. Gaster, A note on the relation between temporally - increasing and spatially - increasing disturbances in hydrodynamic stability, J. Fluid Mech. 14 (1962) 222-224.
[34] S. Chandrasekhar, Hydrodynamic and Hydromagnetic Stability, Dover Publications, New York, 1981.
[35] M. F. El-Sayed, Electrohydrodynamic instability of two superposed Walters B' viscoelastic fluids in relative motion through porous medium, Arch. Appl. Mech. 71 (2001) 717-732.
[36] M. F. El-Sayed, G. M. Moatimid, F. M. F. Elsabaa, M. F. E. Amer, Electrohydrodynamic instability of a non-Newtonian dielectric liquid jet moving in a streaming dielectric gas with a surface tension gradient, Atom. & Sprays 26 (2016a) 349–376.
[37] M. F. El-Sayed, G. M. Moatimid, F. M. F. Elsabaa, M. F. E. Amer, Axisymmetric and asymmetric instabilities of a non-Newtonian liquid jet moving in an inviscid streaming gas through porous media, J. Porous Med. 19 (2016b) 751-769.
[38] M. F. El-Sayed, G. M. Moatimid, F. M. F. Elsabaa, M. F. E. Amer, Three-dimensional instability of non-Newtonian viscoelastic liquid jets issued into a streaming viscous (or inviscid) gas, Int. J. Fluid Mech. Res. 44 (2017) 93-113.